Preprint typeset in JINST style - HYPER VERSION

Addendum–2 to the CAN–037 note on the first results of the SDHCAL technological prototype

CALICE collaboration.

ABSTRACT: In this addendum, a new analysis of the data collected during the SDHCAL prototype exposure to pion beam at the H6 beam line of the CERN-SPS in September 2012 is presented. The analysis is extended to include the data collected at the H2 SPS beam line as well. The selection of the pion sample in this analysis differs from that presented in the CAN–037 note. The new selection is based on more simple criteria that were detailed in addendum-1 of the same note. The resolution found with the present analysis is improved with respect to the one presented in addendum-1. The improvement is notable for hadronic showers of high energy (> 30 GeV). This improvement is obtained by applying a calibration method that takes into account the degradation of the GRPC response for runs with rather high particle beam rate.

Contents

1. Introduction

In order to validate the SDHCAL technology, the prototype was exposed to muons, pions and electrons of the CERN H6 beam line of the SPS in September 2012, and of the H2 beam line in November 2012. In the current addendum we show reanalysis of the same set of events collected during the September 2012 campaign and presented in the CAN–037 note and the associated addendum-1. Also we show here the results of the new analysis of the data taken during November 2012 runs. In both cases to avoid efficiency loss in the GRPC in case of high particle rate only runs with less than 1000 particles per spill were studied. The detailed explanation of hadronic shower selection can be found in addendum–1 to the note CAN–037.

2. Spill time correction

Even though the beam parameters during the two data taking periods were optimized to get spills containing less than 1000 particles it was observed that for some runs of both periods the number of hits associated to hadronic showers was decreasing during the spill time. The decrease is more apparent for the number of hits associated to the second and third thresholds of the semi-digital readout as can be shown in Figure 1. The effect is more frequent in runs of high energy pions. The consequence of such behavior is a degradation of hadronic showers energy resolution. In order to correct for the effect, two special calibration techniques were developed. The first one is a linear fit calibration. The average number of hits associated to each threshold of each hadronic shower is plotted as a function of their time occurrence within a spill. Then a linear fit to the hit distributions is performed and the slope of the fit is determined. The corrected number of hits N_{corr} for each run and for each threshold i is defined according to the following formula:

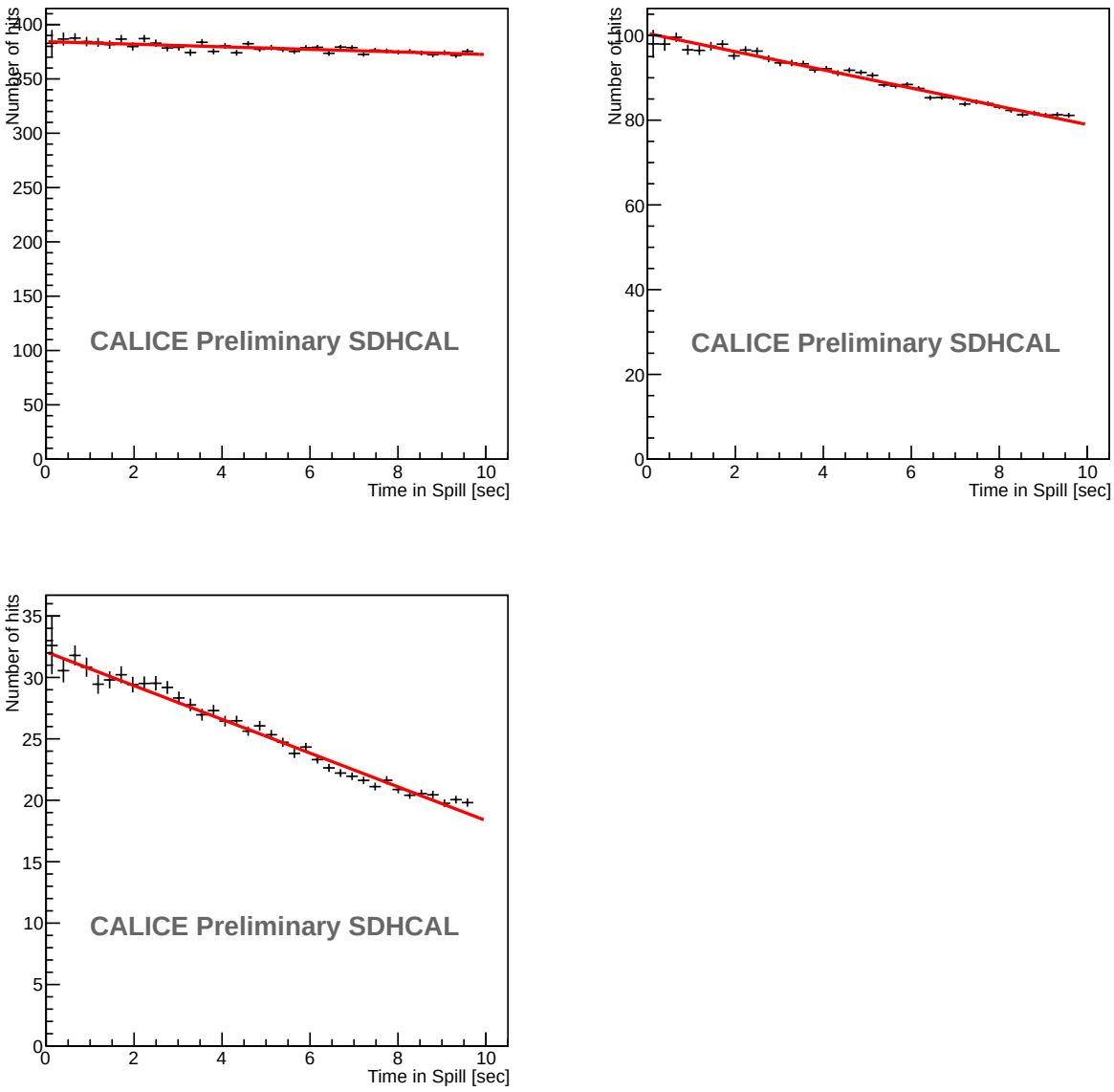

Figure 1. Number of hits as a function of spill time for 3 different thresholds at 30 GeV run from September.

$$N_{corr} = \sum_{i=1}^{3} Nhit_i - slope_i * TimeInSpill \tag{2.1}$$

where $Nhit_i$ is the number of hits of a given threshold i at the beginning of the spill and $TimeInSpill$ is the occurrence time within the spill. The results before and after the linear fit calibration for 80 GeV run from September data can be seen in Figure 2. The alternative way of doing the correction is a time slots calibration. For each run and each threshold, the spill time was divided by 5 slots.

Then a gaussian fit was performed for each of the number of hits distribution of each threshold for each time slot separately as shown in Figure 3. The mean value from the fit for the first distribution (at the beginning of the spill) was taken as a reference. The correction factors for other 4 time slots are defined as $coeff_i = mean_1/mean_i$. The corrected number of hits N_{corr} for each threshold is then defined as following:

$$N_{corr} = \sum_{i=1}^{5} Nhit_i * coeff_i \tag{2.2}$$

As shown in Figures 2 and 4 both types of calibration are able to correct for the spill time effect. We observed that the energy resolution is slightly better for linear fit calibration however the linearity was found to be a little worse in this case. Finally the lack of statistics for some runs led us to choose the linear fit calibration as the default one for both September and November data samples.

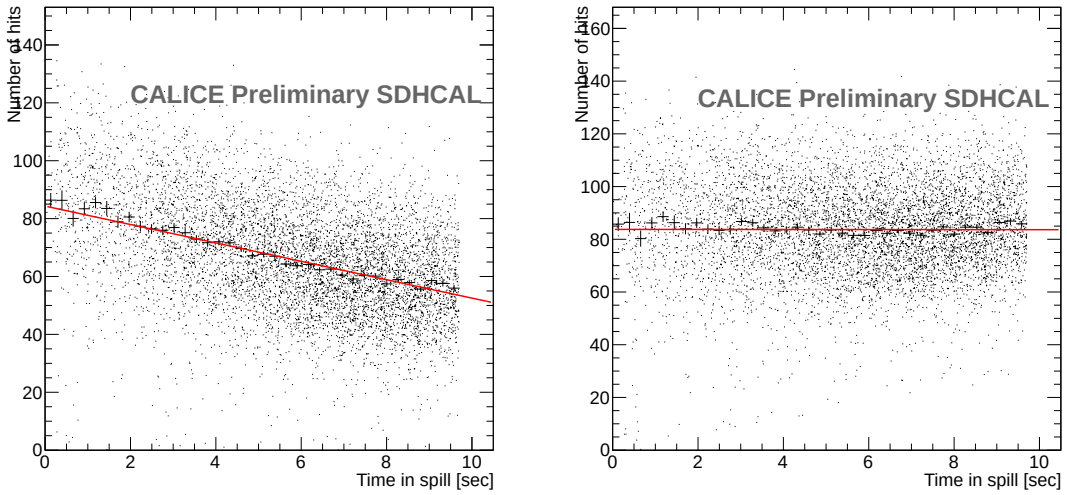

Figure 2. Number of hits for the third threshold 80 GeV run as a function of spill time before (left) and after (right) linear fit calibration.

3. Results

After applying the selection described in addendum-1, an extension of the procedure presented in [1] section 4.2 is used to determine the reconstructed energy of hadronic showers. In the extended procedure the energy is given by the following equation:

$$E_{reco} = \alpha(N_{tot})N_1 + \beta(N_{tot})N_2 + \gamma(N_{tot})N_3 + cN_{HT} \tag{3.1}$$

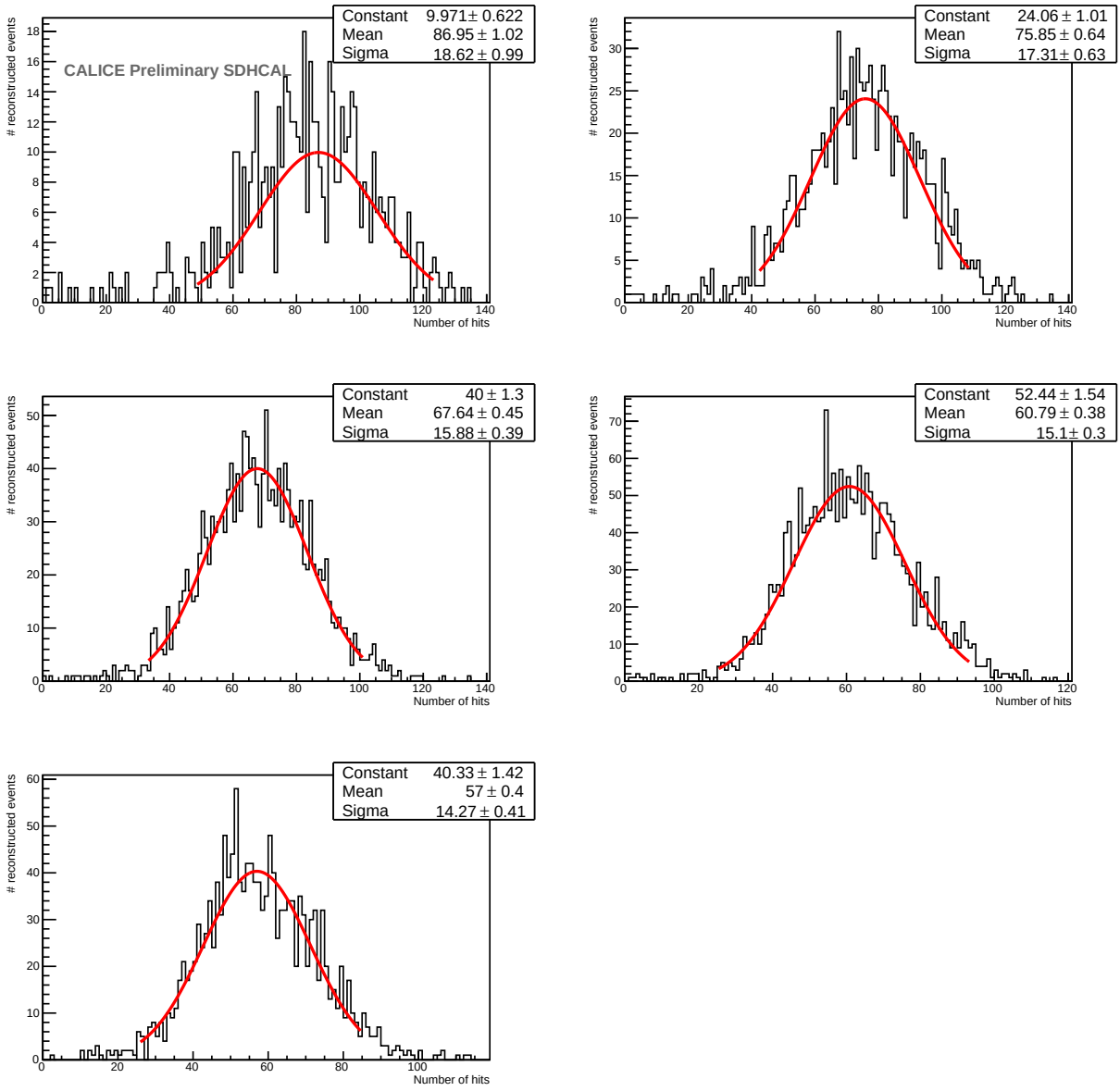

Figure 3. Hit distributions for five different time slots in spill with a step of 2 seconds. The Gaussian fit is shown as a red line.

where N_{HT} is the number of hits belonging to the segments of the hadronic shower selected using the Hough Transform method as explained in [2]. N_i are the number of remaining hits associated to the i^{th} threshold. α, β, γ, are quadratic functions of the total number of hits N_{tot} and c is a constant coefficient that reflects the fact that the HT segments are essentially produced by mips. The presence of high thresholds in these segments is either a fluctuation or the result of large dE/dx at the stopping end and in both cases this has not the same signification as the thresholds associated to the hits present in the dense part of the shower. Therefore all the hits belonging to

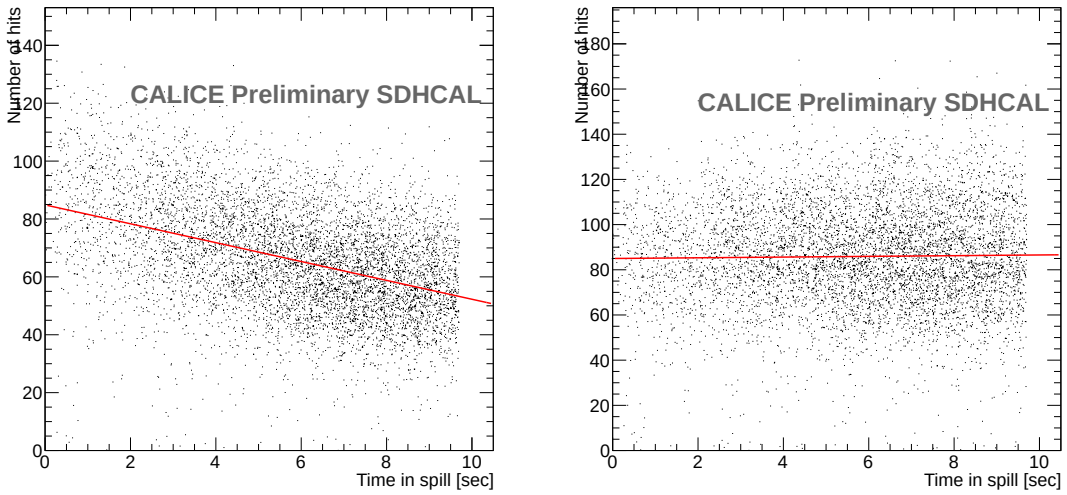

Figure 4. Number of hits for the third threshold 80 GeV run as a function of spill time before (left) and after (right) time slots calibration.

such segments are given the same weight. As in the previous note, the ten parameters (there are nine in the previous analysis) are optimized using a part of of September data of only few energy points. The coefficients are obtained from a χ^2 minimization using some of the energy bins:

$$\chi^2 = \sum_{i=1}^{N} \frac{(E^i_{beam} - E^i_{reco})^2}{E^i_{beam}} \tag{3.2}$$

These coefficients are then used to estimate the energy of incoming particles. The reconstructed energy distributions were fitted with the two-step Gaussian fit. First, a Gaussian was used to fit over the full range of the distribution. Second, a Gaussian was fitted only in the range of $\pm 1.5\sigma$ of the first fit. The σ of second fit was used for the energy resolution estimation. The Crystal Ball function fit defined in [1] (Appendix A) was also performed. The difference of the two fits is used as the systematics error. A full systematics study will be performed in the future.

The linearity and energy resolution of the two sets of data are presented in Figures 5, 6 and 7, 8. The improvement of the September data with respect to the results presented in addendum-1 is obvious at high energy. This improvement in energy resolution is as high as 20% in some cases.

The results obtained with the two data samples with the same energy points are in remarkable agreement and show clearly that the behavior of SDHCAL prototype is stable between the two periods as it can be seen in Figure 9 .

Another attempt to improve the energy resolution was tried. In addition to singling out the so-called Hough Transform hits, it consists of separating the remaining hits of a hadronic shower into high-density part and low-density part. The first is essentially the electromagnetic part while the second is the hadronic part. A different energy weight function is then applied to each part.

To determine the hits belonging to the low or to the high-density parts, for each hit the number of other hits located at a distance smaller than 1.5 cm in x and in y directions and smaller than 3.1 cm in z direction is considered. The distances are being defined by the geometry of SDHCAL prototype. Figure 10 shows hit density distributions for pions and for electrons at 50 GeV and 20 GeV runs after excluding muons as it presented in addendum–1. The intersection point at density=9 indicates the cut which separates the low-density and the high-density parts of the hadronic shower. The intersection point depends a little with energy. Therefore the study for different density cuts were done. The effect on energy resolution and linearity was found almost negligible. The energy of the hadronic shower is then expressed as follows:

$$E_{reco} = \alpha_h(N_{tot})N_{h1} + \beta_h(N_{tot})N_{h2} + \gamma_h(N_{tot})N_{h3} + \alpha_l(N_{tot})N_{l1} + \beta_l(N_{tot})N_{l2} + \gamma_l(N_{tot})N_{l3} + cN_{HT} \tag{3.3}$$

where $\alpha_h, \beta_h, \gamma_h, \alpha_l, \beta_l, \gamma_l$, are quadratic functions of total number of hits N_{tot}, N_{hi} and N_{li} are the number of hits for the i^{th} threshold for high and for low-density parts of the hadronic shower. A new fit of the 19 parameters is performed following the previous recipe. The best value of $c = 0.032$ was found after optimization of the parameters. It is a little lower compare to $c = 0.045$ which corresponds to the 10 parameters case.

Figures 11 and 12 show the mean reconstructed energy for pion showers versus the beam energy and the relative deviation to the beam energy for September and November data respectively. The parameters used for energy reconstruction were optimized with September data set only. Application of those parameters to November data set (where beam conditions are different) shows acceptable agreement which is demonstrated in Figure 12.

Figures 13 and 14 show the energy resolution as a function of the beam energy defined as $\frac{\sigma}{E_{beam}}$ where σ is calculated from two-step Gaussian fit. All these results are summarized in the Tables A, B, C and D and plots 15, 16. There is no significant improvement in energy resolution for reconstruction method with 19 parameters compare to the parameterisation with 10. Partially it can be explained by the fact that quadratic function procedure has already reached the limit and can't be improved further on. However the work is ongoing and more enhancements are expected from the extention of current method.

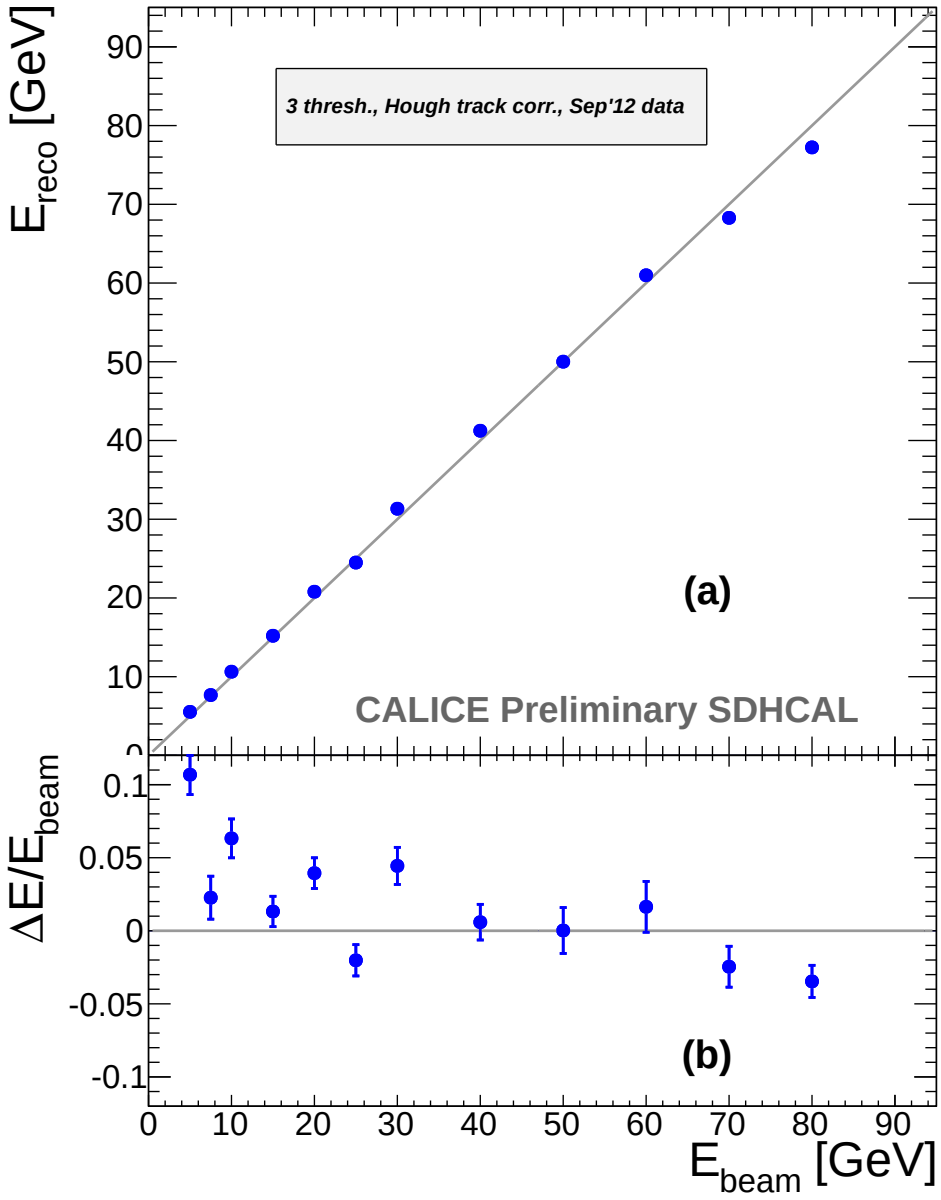

Figure 5. (a): Mean reconstructed energy for pion showers at September runs and (b): relative deviation of the pion mean reconstructed energy with respect to the beam energy as a function of the beam energy.The reconstructed energy is computed using the three thresholds information and the distributions are fitted with a Gaussian. Hough Transform track correction and 10 parameters are used.

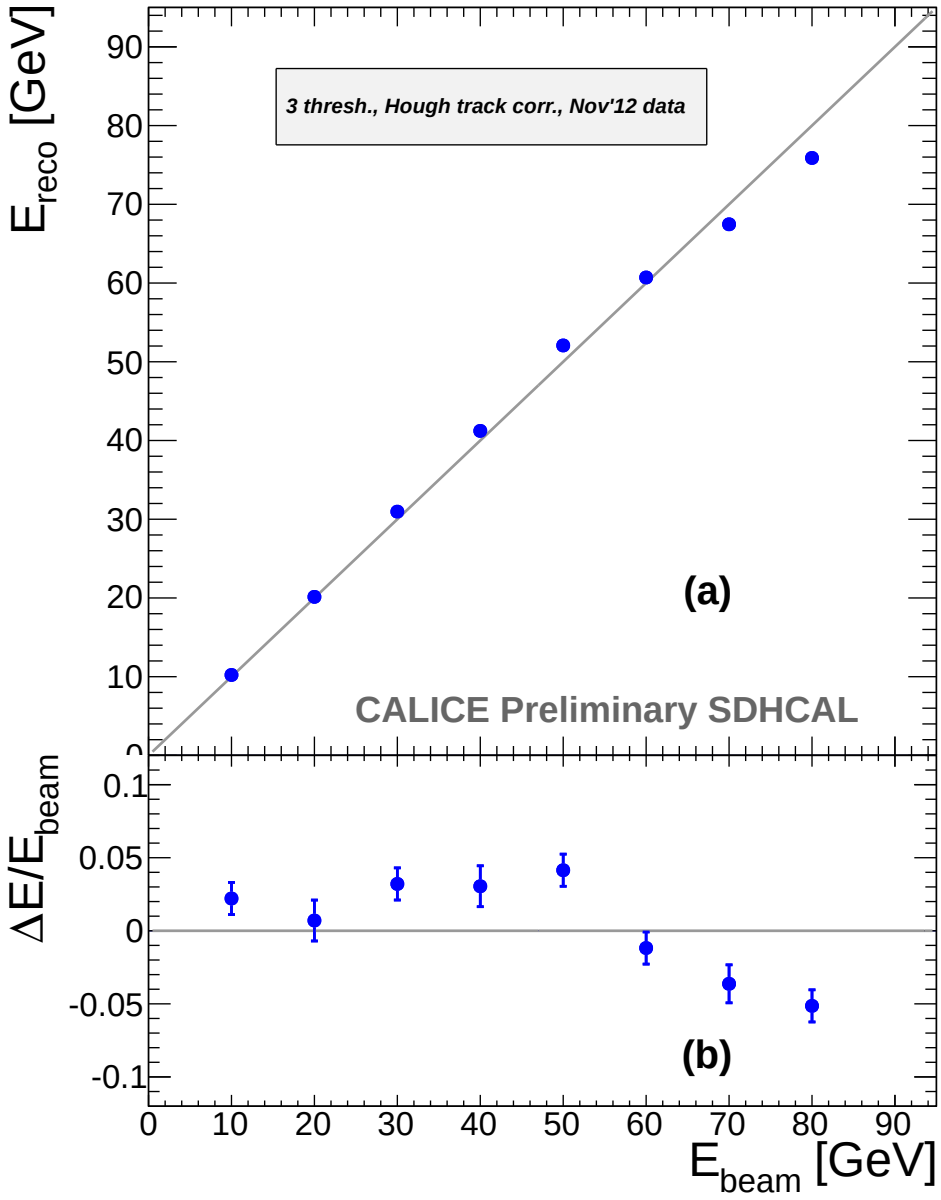

Figure 6. (a): Mean reconstructed energy for pion showers at November runs and (b): relative deviation of the pion mean reconstructed energy with respect to the beam energy as a function of the beam energy.The reconstructed energy is computed using the three thresholds information and the distributions are fitted with a Gaussian. Hough Transform track correction and 10 parameters are used.

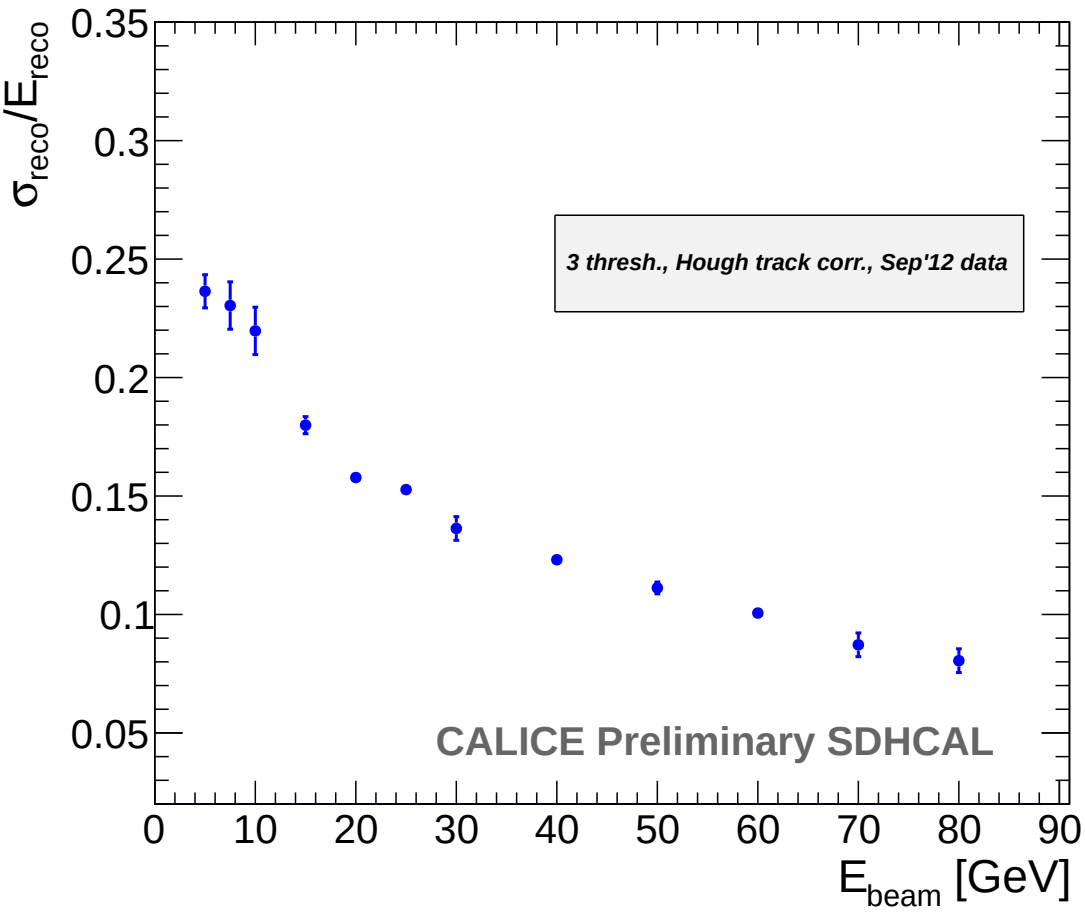

Figure 7. $\frac{\sigma E_{reco}}{E_{reco}}$ of the reconstructed pion energy as a function of the beam energy at September runs. The reconstructed energy is computed using the three thresholds information and the distributions are fitted with a Gaussian. Hough Transform track correction and 10 parameters are used.

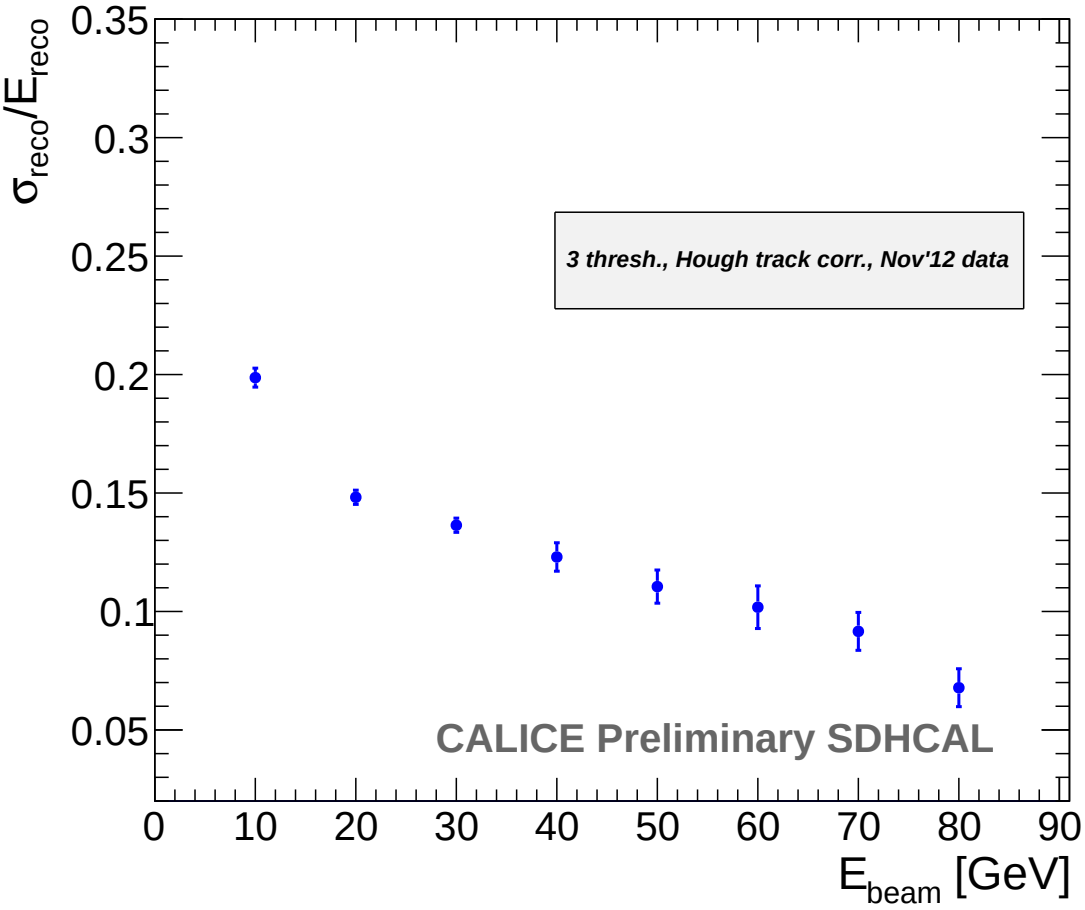

Figure 8. $\frac{\sigma E_{reco}}{E_{reco}}$ of the reconstructed pion energy as a function of the beam energy at November runs. The reconstructed energy is computed using the three thresholds information and the distributions are fitted with a Gaussian. Hough Transform track correction and 10 parameters are used.

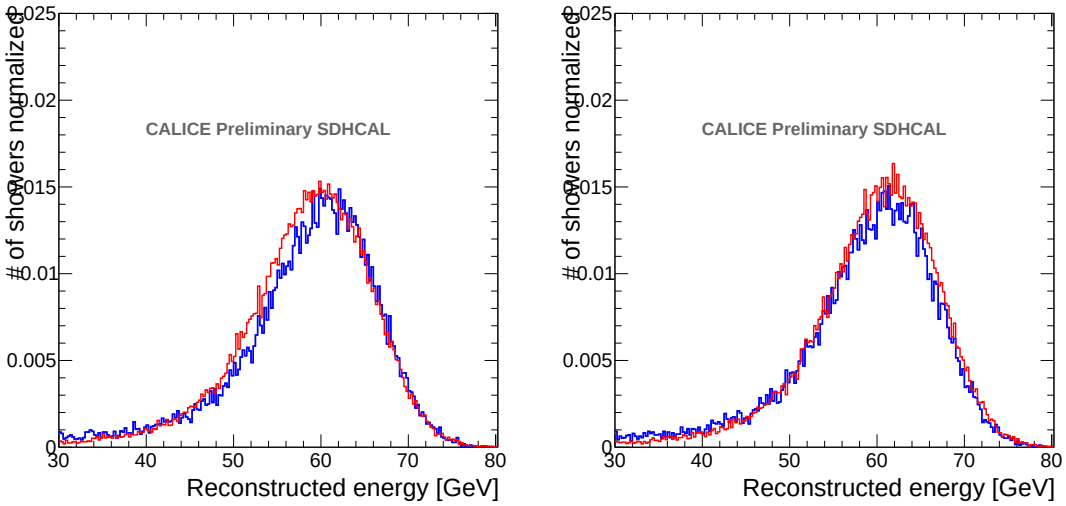

Figure 9. Reconstructed energy distributions for September (red line) and November (blue line) 60 GeV runs before (left) and after (right) spill time correction.

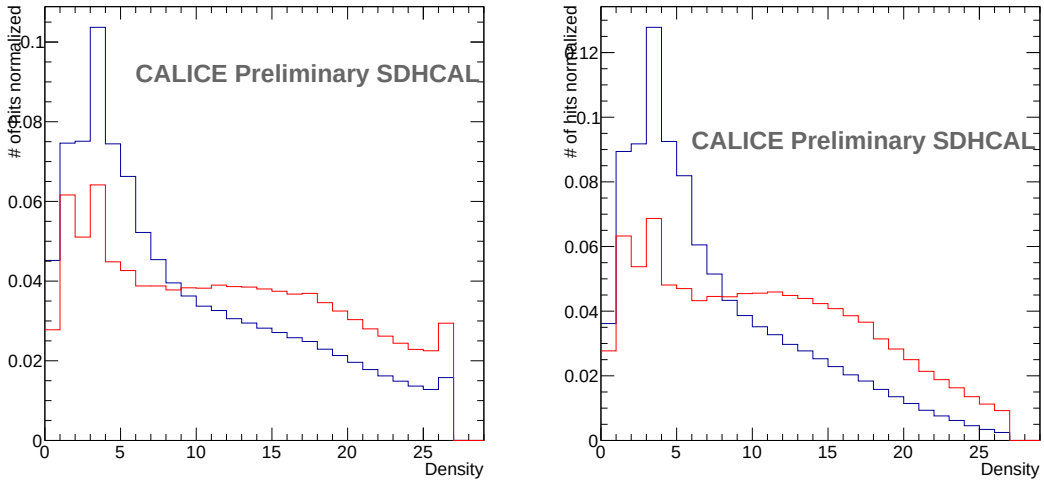

Figure 10. Hit density distributions for pions (blue line) and for electrons (red line) at 50 GeV (left) and 20 GeV (right) runs.

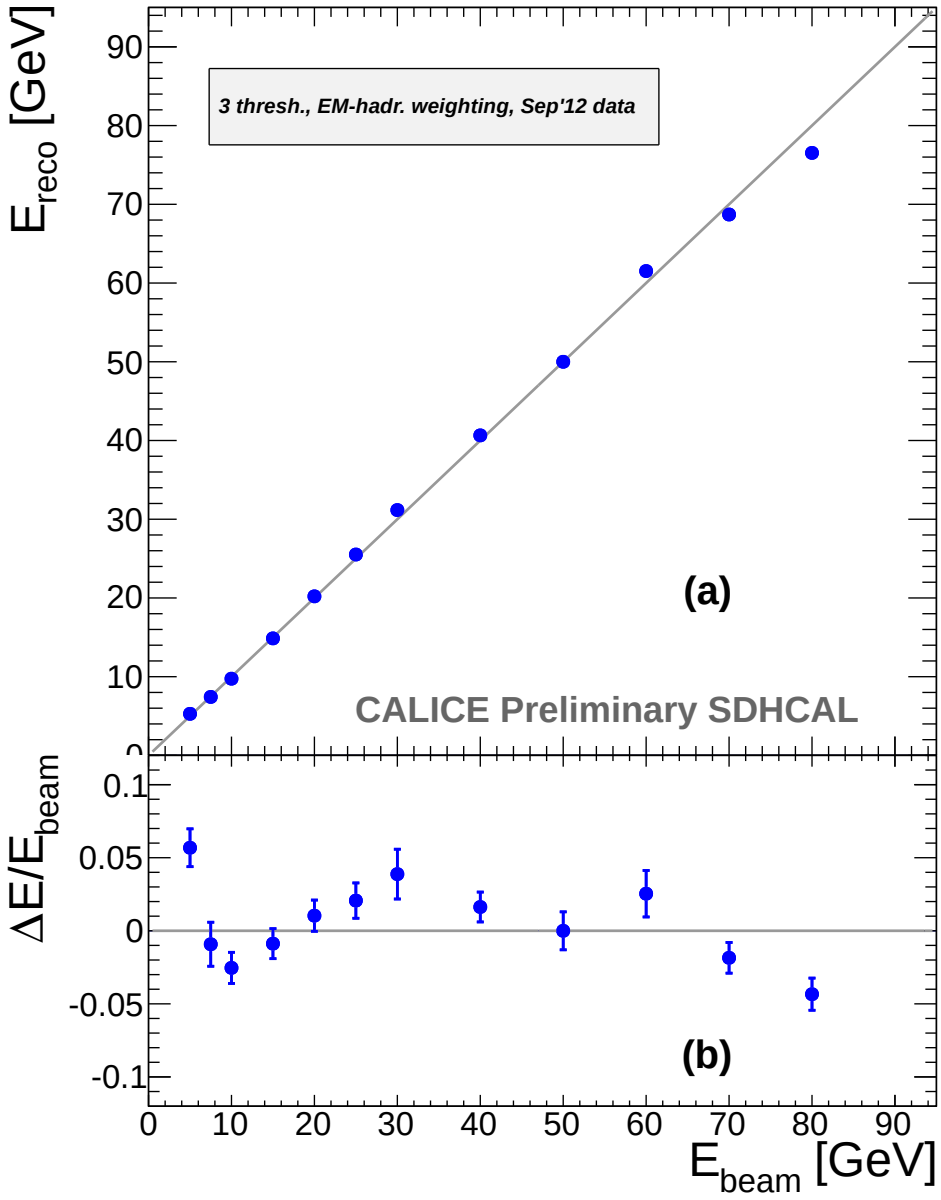

Figure 11. (a): Mean reconstructed energy for pion showers at September runs and (b): relative deviation of the pion mean reconstructed energy with respect to the beam energy as a function of the beam energy.The reconstructed energy is computed using the three thresholds information and the distributions are fitted with a Gaussian. 19 parameters are used.

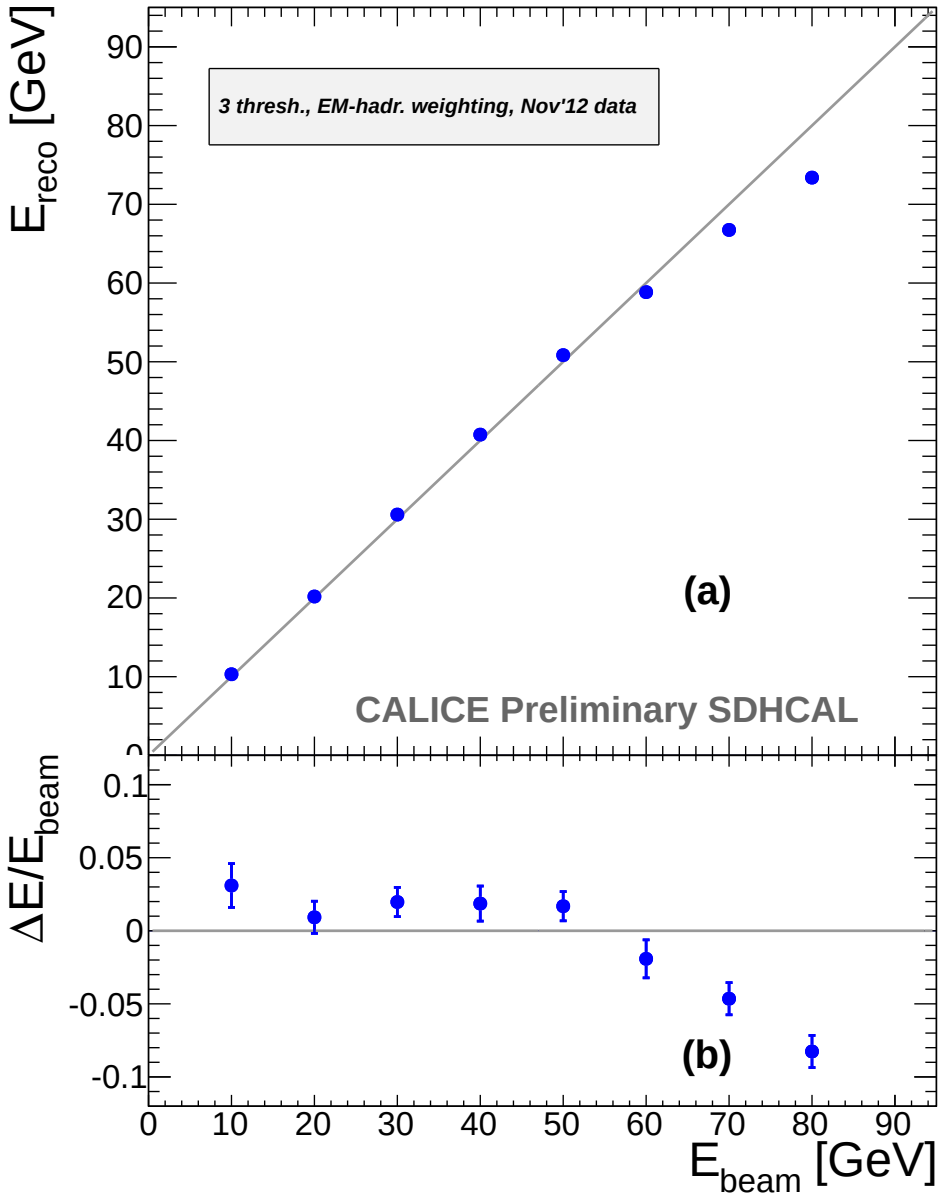

Figure 12. (a): Mean reconstructed energy for pion showers at November runs and (b): relative deviation of the pion mean reconstructed energy with respect to the beam energy as a function of the beam energy.The reconstructed energy is computed using the three thresholds information and the distributions are fitted with a Gaussian. 19 parameters are used.

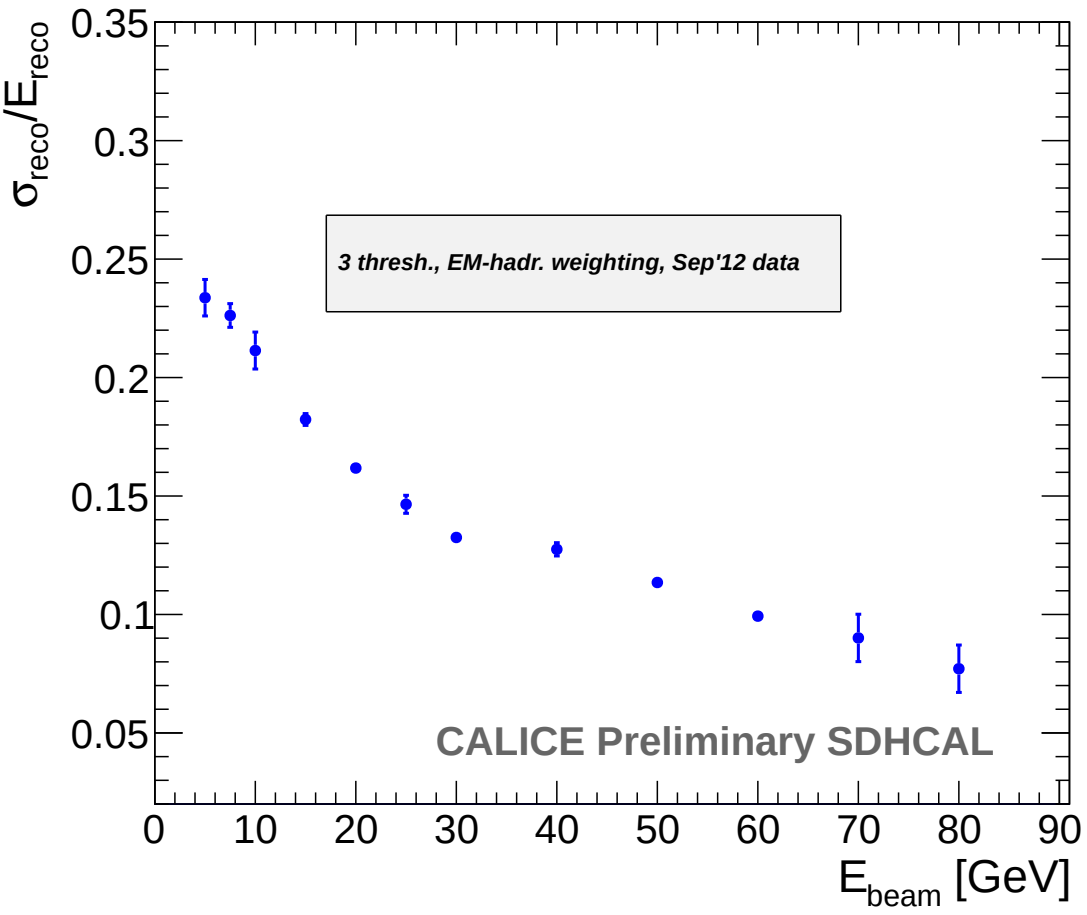

Figure 13. $\frac{\sigma E_{reco}}{E_{reco}}$ of the reconstructed pion energy as a function of the beam energy at September runs. The reconstructed energy is computed using the three thresholds information and the distributions are fitted with a Gaussian. 19 parameters are used.

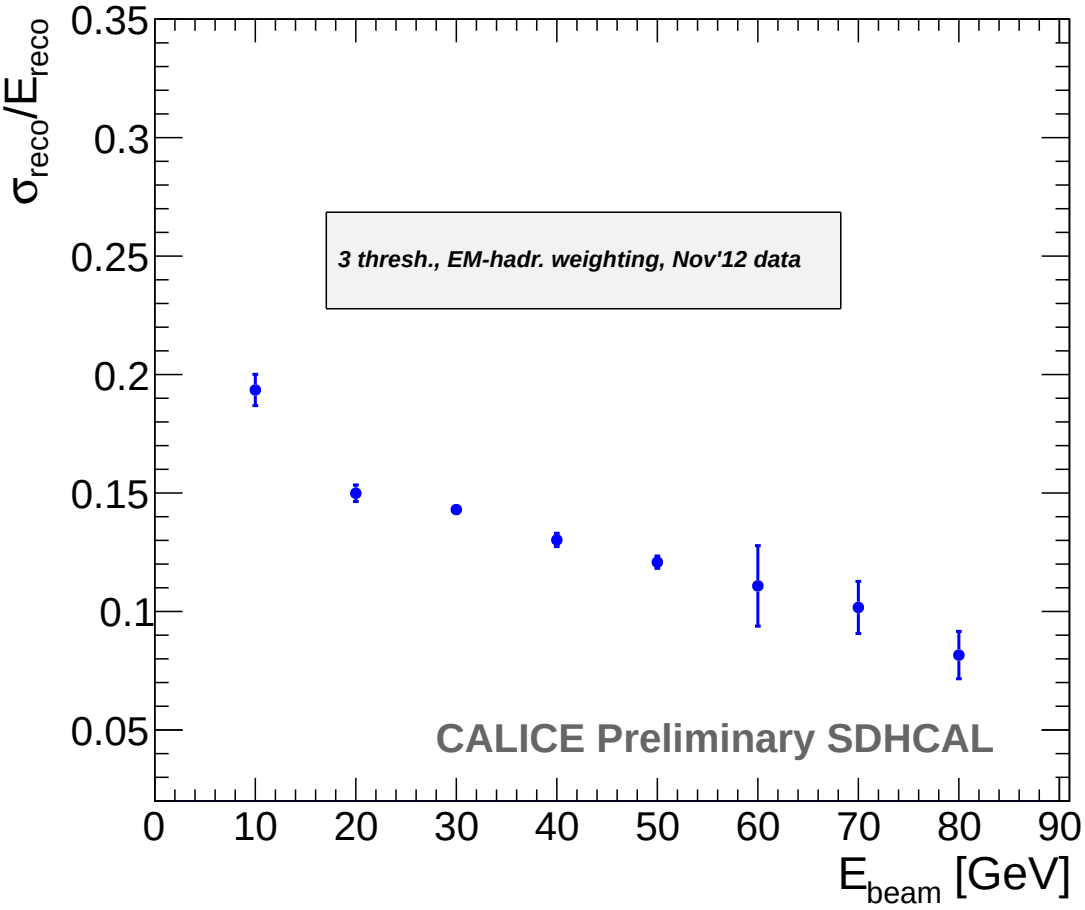

Figure 14. $\frac{\sigma E_{reco}}{E_{reco}}$ of the reconstructed pion energy as a function of the beam energy at November runs. The reconstructed energy is computed using the three thresholds information and the distributions are fitted with a Gaussian. 19 parameters are used.

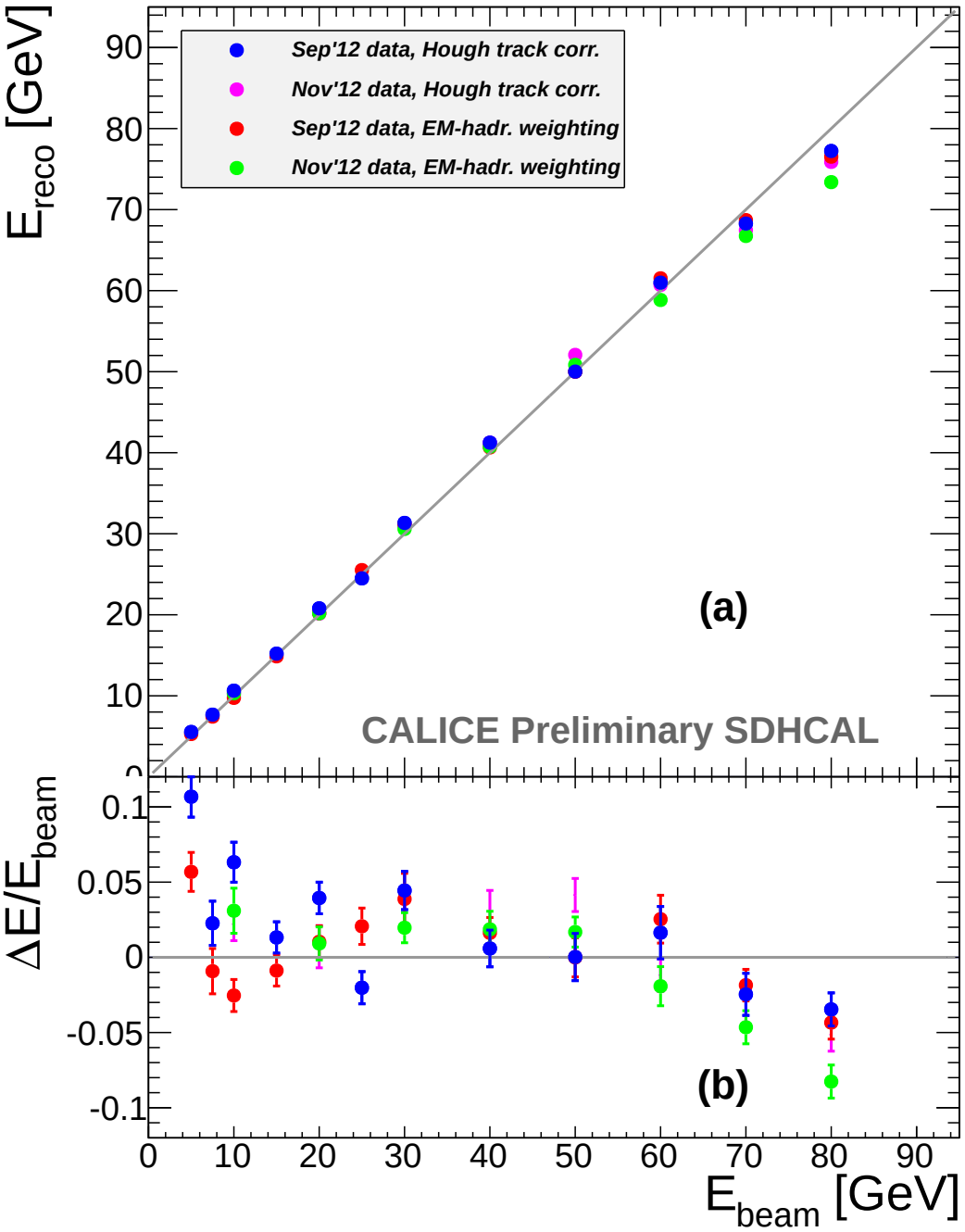

Figure 15. (a): Mean reconstructed energy for pion showers and (b): relative deviation of the pion mean reconstructed energy with respect to the beam energy as a function of the beam energy.The reconstructed energy is computed using the three thresholds information and the distributions are fitted with a Gaussian. Blue points represent September 10 parameters data, magenta points – November 10 parameters data, red – September 19 parameters data and green – November 19 parameters data.

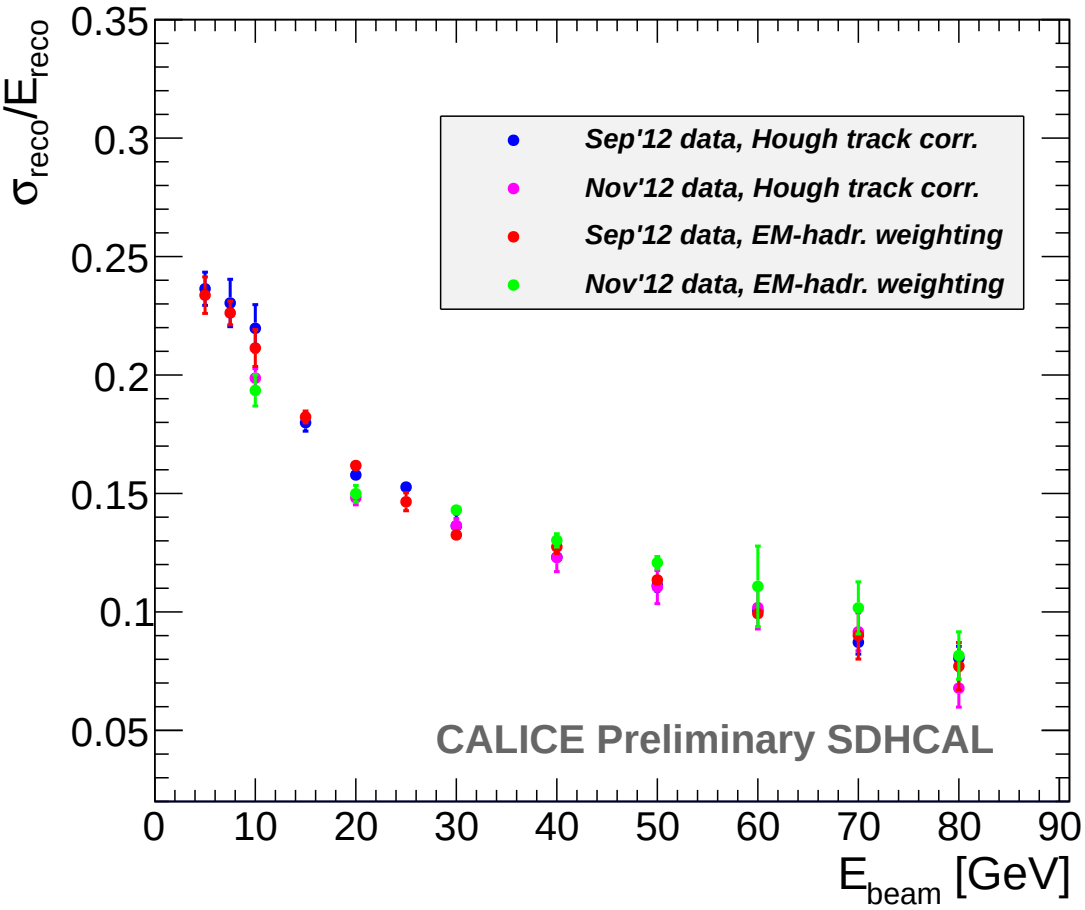

Figure 16. $\frac{\sigma E_{reco}}{E_{reco}}$ of the reconstructed pion energy as a function of the beam energy. The reconstructed energy is computed using the three thresholds information and the distributions are fitted with a Gaussian. Blue points represent September 10 parameters data, magenta points – November 10 parameters data, red – September 19 parameters data and green – November 19 parameters data.

4. Conclusion

The results obtained with this new analysis confirm those presented in the CAN–037 note. Applying of Hough Transform technique allowes to improve energy resolution by few percent for all energy bins. The further improvement on resolution at high energy is due to the spill time correction effect.

References

[1] The CALICE Collaboration, *First results of the CALICE SDHCAL technological prototype*, CALICE Analysis Note CAN–037.

[2] The CALICE Collaboration, *Tracking within Hadronic Showers in the SDHCAL prototype using Hough Transform Technique* , CALICE Analysis Note CAN–047.

A. Result summary 1

$E_{beam}(GeV)$	$E_{reco}(GeV)$	$\frac{\Delta E}{E_{beam}}(\%)$	$\frac{\sigma E_{reco}}{E_{reco}}(\%)$
5	5.534 ± 0.03	10.7 ± 1.4	23.6 ± 0.7
7.5	7.669 ± 0.03	2.3 ± 1.5	23.0 ± 1.0
10	10.63 ± 0.02	6.3 ± 1.3	21.9 ± 1.1
15	15.19 ± 0.02	1.3 ± 1.0	17.9 ± 0.4
20	20.79 ± 0.02	3.9 ± 1.0	15.8 ± 0.1
25	24.49 ± 0.02	-2.0 ± 1.1	15.3 ± 0.1
30	31.33 ± 0.03	4.4 ± 1.3	13.6 ± 0.5
40	41.24 ± 0.03	0.6 ± 1.2	12.3 ± 0.1
50	50.01 ± 0.07	0.0 ± 1.6	11.2 ± 0.2
60	60.99 ± 0.04	1.6 ± 1.7	10.0 ± 0.1
70	68.28 ± 0.04	-2.5 ± 1.4	8.7 ± 0.6
80	77.23 ± 0.04	-3.5 ± 1.4	8.0 ± 0.6

Table 1. Mean reconstructed energy E_{reco}, relative deviation to the beam energy $\frac{\Delta E}{E_{beam}}$ and energy resolution $\frac{\sigma E_{reco}}{E_{reco}}$ at September runs quoted in %. Energy is reconstructed with 10 parameters.

B. Result summary 2

$E_{beam}(GeV)$	$E_{reco}(GeV)$	$\frac{\Delta E}{E_{beam}}(\%)$	$\frac{\sigma E_{reco}}{E_{reco}}(\%)$
10	10.22 ± 0.05	2.2 ± 1.1	19.9 ± 0.4
20	20.14 ± 0.02	0.7 ± 1.4	14.8 ± 0.3
30	30.96 ± 0.04	3.2 ± 1.1	13.6 ± 0.3
40	41.22 ± 0.04	3.0 ± 1.4	12.3 ± 0.6
50	52.01 ± 0.12	4.1 ± 1.1	11.0 ± 0.7
60	60.70 ± 0.05	-1.1 ± 1.1	10.2 ± 0.9
70	67.46 ± 0.04	-3.6 ± 1.3	9.1 ± 0.8
80	75.89 ± 0.04	-5.1 ± 1.3	6.8 ± 0.8

Table 2. Mean reconstructed energy E_{reco}, relative deviation to the beam energy $\frac{\Delta E}{E_{beam}}$ and energy resolution $\frac{\sigma E_{reco}}{E_{reco}}$ at November runs quoted in %. Energy is reconstructed with 10 parameters.

C. Result summary 3

$E_{beam}(GeV)$	$E_{reco}(GeV)$	$\frac{\Delta E}{E_{beam}}(\%)$	$\frac{\sigma E_{reco}}{E_{reco}}(\%)$
5	5.284 ± 0.02	5.7 ± 1.3	23.4 ± 0.8
7.5	7.431 ± 0.03	-0.9 ± 1.5	22.6 ± 0.5
10	9.746 ± 0.02	-2.5 ± 1.1	21.1 ± 0.8
15	14.87 ± 0.02	-0.9 ± 1.0	18.2 ± 0.3
20	20.21 ± 0.02	1.0 ± 1.1	16.2 ± 0.1
25	25.51 ± 0.02	2.1 ± 1.2	14.7 ± 0.4
30	31.16 ± 0.03	3.9 ± 1.7	13.3 ± 0.2
40	40.65 ± 0.03	1.6 ± 1.0	12.8 ± 0.3
50	50.00 ± 0.07	0.0 ± 1.3	11.4 ± 0.2
60	61.52 ± 0.04	2.5 ± 1.6	9.9 ± 0.1
70	68.70 ± 0.04	-1.9 ± 1.1	9.0 ± 1.0
80	76.53 ± 0.04	-4.3 ± 1.1	7.7 ± 1.0

Table 3. Mean reconstructed energy E_{reco}, relative deviation to the beam energy $\frac{\Delta E}{E_{beam}}$ and energy resolution $\frac{\sigma E_{reco}}{E_{reco}}$ at September runs quoted in %. Energy is reconstructed with 19 parameters.

D. Result summary 4

$E_{beam}(GeV)$	$E_{reco}(GeV)$	$\frac{\Delta E}{E_{beam}}(\%)$	$\frac{\sigma E_{reco}}{E_{reco}}(\%)$
10	10.31 ± 0.04	3.1 ± 1.5	19.4 ± 0.6
20	20.18 ± 0.02	0.9 ± 1.1	14.9 ± 0.4
30	30.59 ± 0.04	1.9 ± 1.0	14.3 ± 0.2
40	40.74 ± 0.04	1.9 ± 1.2	13.0 ± 0.3
50	50.84 ± 0.04	1.7 ± 1.0	12.1 ± 0.3
60	58.85 ± 0.06	-1.9 ± 1.3	11.1 ± 1.7
70	66.75 ± 0.04	-4.6 ± 1.1	10.2 ± 1.1
80	73.39 ± 0.04	-8.3 ± 1.1	8.2 ± 1.0

Table 4. Mean reconstructed energy E_{reco}, relative deviation to the beam energy $\frac{\Delta E}{E_{beam}}$ and energy resolution $\frac{\sigma E_{reco}}{E_{reco}}$ at November runs quoted in %. Energy is reconstructed with 19 parameters.